Light Higgs Boson Signal at LHC in the Reaction $pp \to \gamma\gamma + lepton$

M.N. Dubinin, V.A. Ilyin and V.I. Savrin
Institute of Nuclear Physics, Moscow State University, Moscow
Russia

Abstract

We discuss the SM Higgs discovery potential of the LHC in the channel $pp \to H + W/H + t\bar{t} \to \gamma\gamma + lepton$ when the lepton is observed at sufficiently high p_t and a small rapidity to be reliably identified. We calculate all the signal subprocesses and the irreducible background with realistic kinematical cuts. The reducible background is also considered.

We conclude that with an integrated luminosity of 165 fb^{-1} in both channels $pp \to W + H$ and $pp \to t + \bar{t} + H$ about 100 signal events with less than 20 events of the background could be observed in the case of low photon transverse momentum cuts $p_t > 20$ GeV. For the high photon transverse momentum cuts $p_t > 40$ GeV about 50 signal events are expected practically free from the background. At a low luminosity only few clean signal events are expected.

1 Introduction

It is difficult to observe a signal of the light Higgs boson ($M_H < 140$ GeV) at the LHC collider in the inclusive channel $pp \to \gamma\gamma + X$ [1, 2]. The irreducible backgrounds from the $q\bar{q} \to \gamma\gamma$ and $gg \to \gamma\gamma$ subprocesses are large and for rather small $\gamma\gamma$ pair invariant masses the *signal/background* ratio is in the best case 1/10. In this situation it is important to understand whether we can observe at the LHC any other Higgs boson production mechanisms. In the following we are considering the Higgs discovery potential in the channel $pp \to \gamma\gamma + lepton$ when the lepton is observed at a sufficiently high transverse momentum and small rapidity to be reliably identified. In this channel the signal cross section is much smaller in comparison with the inclusive $pp \to \gamma\gamma + X$ case, but the *signal/background* ratio can be very large and the background does not play so important role. Similar to the $\gamma\gamma + jet$ channel, transition to larger p_t allows us to reduce the overwhelming backgrounds of the completely inclusive channel mentioned above. The isolated energetic lepton from the W or t decays gives additional possibilities to separate the backgrounds. Reconstruction of the charged lepton track makes possible to indicate precisely the primary vertex position, which is important in the high luminosity LHC regime.

The idea to look for the Higgs boson signal associated with a high p_t lepton has some history. The reactions $pp \to H + W$ (for the channel $H \to b\bar{b}$) and $pp \to t + \bar{t} + H$ were considered in [3] and [4], respectively. First calculations for the $\gamma\gamma + lepton$ final state with a complete tree level set of diagrams for the irreducible background were carried out in [5, 6]. In these papers slightly different detector cuts were used in comparison with [2] for collider energy $\sqrt{s}$ =16 TeV. It was pointed out that a careful analysis of various misidentification backgrounds should be performed. A more recent study involving some misidentification backgrounds has been presented in [7]. Detailed complementary discussion of the misidentification backgrounds for the SSC energy $\sqrt{s}$ =40 TeV can be found in [8]. In this paper we are trying to present more extended and updated analysis of the signal and background processes with the final state $\gamma\gamma + lepton$ at LHC.

We calculated cross sections and distributions with the help of the CompHEP package [9][1] which allows to calculate squared matrix elements corresponding to the complete set of SM tree level diagrams for considered processes and perform the convolution with parton distributions. The subsequent adaptive multichannel Monte Carlo integration with various sets of kinematical cuts allows one to realize some optimisation of cuts ensuring a better separation of signal. In all cases we used an advanced facility of the CompHEP package worked out to regularize sharp peaks of the amplitude [10]. Note that the vertex ggH in the signal QCD diagrams, including quark loops, was implemented in CompHEP as an effective point-like vertex together with the $gggH$ vertex to ensure gauge inivariance of the amplitude.

The CompHEP package includes the code of adaptive MC integrator VEGAS [11]. For parton distribution functions we used the parametrizations CTEQ3m [12], CTEQ4m and CTEQ4l [13], MRS-A' [14] and GRV92 (HO) [15]. The corresponding codes are also implemented in CompHEP.

[1] CompHEP package is distributed freely. The codes are available at *http://theory.npi.msu.su*.

The paper is organized as follows. In Section 2 we list the values of physical parameters and some physical conventions.

In Section 3 we study the reaction $pp \to \gamma\gamma + lepton$. We discuss a calculation of the signal process $pp \to W + H \to \gamma\gamma + e\nu_e$ and the irreducible background in Section 3.1. Optimisation of kinematical cuts is considered in detail. Results for the signal process $pp \to t + \bar{t} + H \to t\bar{t} + \gamma\gamma$ and the irreducible background are described in Section 3.2. Various misidentification backgrounds are discussed in Sections 3.3-3.6. In particular these are the backgrounds when a quark or gluon jet is misidentified as a photon, the b-quark is misidentified as an electron and, maybe, the electron is misidentified as a photon. In Section 4 a summary for the reaction $pp \to \gamma\gamma + lepton$ is presented.

2 Input parameters and physical conventions

Exactly as in the case of $\gamma\gamma+jet$ channel [16] in our calculations we used $\sqrt{s} = 14$ TeV and $M_Z = 91.1884$ GeV, $\sin^2\theta_w = 0.2238$. For heavy quark masses we took the values $m_s = 0.2$ GeV, $m_c = 1.3$ GeV, $m_b = 4.3$ GeV and $m_t = 175$ GeV [17].

For the strong coupling constant we are using the normalization

$$\alpha_s(M_Z) = 0.118,$$

where α_s runs in correspondence with the 2nd order QCD (NLO) formulas with flavour matching (see, e.g., [17], p.77). This normalization assumes that $\Lambda^{(5)}_{QCD} = 226$ MeV. For instance, $\alpha_s(120\text{GeV}) = 0.1133$.

In electroweak vertices we are using $\alpha(M_Z) = 1/128.9$ [17] calculating electroweak couplings and the Fermi constant by means of the corresponding formulas with $\alpha(M_Z)$, M_Z and $\sin^2\theta_w$ as independent parameters. However, it is more accurate to use $\alpha(m_e) = 1/137.036$ in each vertex that includes an on-shell photon because of the absence of photon wave function renormalization in this case. Thus we introduce the correction factor $(128.9/137.036)^2$ for each process with two photons in the final state.

It is well known that in the case when $M_H < 140$ GeV the Higgs boson decays dominantly into a $b\bar{b}$ pair. However, the QCD corrections to this decay partial width are large. So, for reactions where the $H \to \gamma\gamma$ decay occurs it is important to take into account carefully these corrections because they increase the two-photon branching approximately by a factor of 2. Other decay channels related to the $H \to \gamma\gamma$ branching and the effective $\gamma\gamma H$ Lagrangian [18] which can be used for calculation of the partial width $\Gamma_{H\to\gamma\gamma}$ are discussed in detail in [16]

In order to take into account the QCD corrections the NNLO formulas improved by the renormalization group method [19] were proposed for the running quark masses. We implemented in CompHEP the corresponding NLO formulas for the Higgs decay into quarks. This approximation gives results for partial widths higher than the NNLO formulas by $\sim 10\%$ and the corresponding correction factor has been introduced in our computer code.

Electroweak corrections to the Higgs decays into quarks and leptons are small [20] and we neglect them.

Total QCD radiative corrections to the $H \to gg$ partial width can be collected in a factor with value ~ 1.7 [21, 22, 23]. Note that the QCD radiative corrections to the partial width of $H \to \gamma\gamma$ are very small (less than 1%, see, e.g. [22] and references therein).

Electroweak corrections to the partial widths of $H \to \gamma\gamma$ and $H \to gg$ are small and can be neglected [24].

For a precise calculation of the $H \to \gamma\gamma$ branching in the Higgs mass range under consideration one has to account also for the partial width $\Gamma_{H\to WW^*}$, where W^* means the off-shell W-boson 'decaying' into quark or lepton pairs. At the edge of the range ($M_H = 140$ GeV) this branching and the branching to a $b\bar{b}$ pair are of the same order. The corresponding analytical formulas can be found in [25].

All formulas for the partial widths mentioned above and the higher order QCD correction factors were implemented in the CompHEP codes. We checked the numbers obtained for the branching $H \to \gamma\gamma$ by means of CompHEP, PYTHIA 6.1 and the program HDECAY [26] and observed rather good agreement of the results - see [16].

3 Higgs boson signal in the reaction $pp \to \gamma\gamma + lepton$

3.1 Reaction $pp \to \gamma\gamma + e\nu_e$

Associated production of the Higgs boson and a W-boson in the reaction $pp \to WH$ gives final state with two hard photons with invariant mass reconstructing the Higgs mass, a charged lepton and missing transverse momentum. The complete set of tree subprocess diagrams for the process $pp \to \gamma\gamma + e^+\nu_e$ is shown in Fig.1, the set for $pp \to \gamma\gamma + e^-\bar{\nu}_e$ is obtained by charge conjugation. We do not show the quark loop in the $\gamma\gamma H$ vertex but, as in the case of $\gamma\gamma + jet$ final state, it corresponds to the effective point-like interaction (see the effective Lagrangian in [16]). After the convolution with parton distributions the cross section of the subprocess $u\bar{d} \to \gamma\gamma + e^+\nu_e$ is around 1.5 times greater than the $\bar{u}d \to \gamma\gamma + e^-\bar{\nu}_e$ cross section because there are more u-quarks in a proton than d-quarks.

In order to understand better the influence of kinematicalal cuts on the value of the Higgs signal (diagram 9 in Fig.1) we show in Fig. 2 (only for the signal diagram) the distributions in kinematical variables $M_{\gamma\gamma}$, $p_t^{\gamma,e}$, $y_{\gamma,e}$ and the angle between the two photons or a photon and electron when no kinematical cuts are imposed. Standard choice of cuts that was used in the CMS Technical Proposal [2] is the following:

- $p_t^{\gamma_1} > 40$ GeV, $p_t^{\gamma_2} > 20$ GeV, transverse momentum cuts for photons
- $p_t^l > 20$ GeV, transverse momentum cut for electron (or muon)
- $|\eta_{\gamma_{1,2}}| < 2.4$, $|\eta_l| < 2.4$, rapidity cuts for both photons and electron (or muon)
- $\Delta R(\gamma_1, \gamma_2) > 0.3$, $\Delta R(\gamma, l) > 0.3$, isolation cuts for photon or photon-lepton pair.

As usual, $\Delta R = \sqrt{\Delta\varphi^2 + \Delta y^2}$ is the separation between two particles in the φ-y plane. One can see from Fig. 2 that rather many additional signal events in comparison with the case of standard cuts could be observed if we take a larger photon rapidity range, but the limit of 2.4 is fixed by detector geometry. Only a few more events appear if we decrease the p_t cut for photons transverse momentum or the separation cuts $\Delta R_{\gamma\gamma}$, $\Delta R_{e\gamma}$. The separation cuts do not significantly affect the signal. Numerical values of the cross sections for the different sets of kinematical cuts are shown in Table 1.

The results of complete tree level calculations for the signal and irreducible background diagrams of Fig. 1 are shown in Table 2. We present the distributions in invariant mass $M_{\gamma\gamma}$ for the channels $pp \to \gamma\gamma + e^+\nu_e$ and $pp \to \gamma\gamma + e^-\bar{\nu}_e$ in Fig. 3-5. In both channels the irreducible background dangerously increases (see Table 3) when we shift the photon transverse momentum cuts to smaller values (see distributions for the case of $p_t^{\gamma_1} \geq 20$ GeV and $p_t^{\gamma_2} \geq 20$ GeV in Fig. 12). However if we use the transverse momentum cuts slightly larger than the standard [2] 'asymmetric' ones $p_t^{\gamma_1} \geq 40$ GeV and $p_t^{\gamma_2} \geq 20$ GeV (Fig. 4), the background decreases by order of magnitude while the number of signal events only by a factor of two (see the case of $p_t^{\gamma_1} \geq 40$ GeV and $p_t^{\gamma_2} \geq 40$ GeV in Fig. 4). If the muons from $W \to \mu\nu_\mu$ as well as the electrons from $W \to e\nu_e$ are detected, all cross sections (Fig. 3-5) are multiplied by factor 2. Estimated numbers of the signal and irreducible background events in the final states containing electrons and muons are given in Table 1. We did not introduce the efficiency of lepton identification in the detector. It is rather high in all cases, the efficiency of muon identification is slightly better than the efficiency for electrons.

3.2 Reaction $pp \to \gamma\gamma + t\bar{t}$

In the process $pp \to \gamma\gamma + t\bar{t}$ the Higgs boson is radiated from the t-quark. Signal diagrams are shown in Fig. 6. Irreducible background diagrams are the same as shown in Fig. 15 if we replace the b-quark by t-quark. The result of complete tree level calculation is shown in Fig. 7. We have not imposed any cuts for the t-quark, while the cuts for photons are the same as in the process $pp \to \gamma\gamma + l\nu_l$. Numerical values of the cross sections for different p_t cuts are shown in Table 3. At the LHC energy the reaction $pp \to \gamma\gamma + t\bar{t}$ gives approximately as many Higgs signal events as $pp \to \gamma\gamma + l\nu_l$. It is important to notice that if for the latter we can calculate the irreducible background completely, for the former only a primary level of the irreducible background is under control. If we pass, for instance, to the final state

$\gamma\gamma + t\bar{t} \to \gamma\gamma + \bar{b}W^+bW^-$, many additional background diagrams appear and their contribution have not been calculated accurately anywhere.

3.3 Background processes with a quark jet misidentified as a photon: $pp \to \gamma d + e^+\nu_e$, $pp \to \gamma\bar{d} + e^-\bar{\nu}_e$, $pp \to \gamma\bar{u} + e^+\nu_e$, $pp \to \gamma u + e^-\bar{\nu}_e$

In the case of hadronic jet misidentification as a photon these processes could be a source of dangerous (non-interfering) background. The complete set of tree diagrams for the process $gu \to \gamma d + e^+\nu_e$ is shown in Fig. 8. The diagrams for other three reactions can be obtained by obvious replacements of quark species and/or by charge conjugation. The cross sections of these background reactions are of the same order of magnitude (around 10^{-2} pb at the p_t cut of 20 GeV). We show the total rates for several choices of transverse momentum cuts in Table 4. Transverse momentum cut at 40 GeV suppresses the background in the invariant mass distribution by about one order of magnitude in comparison with the case when $p_t \geq 20$ GeV. The distributions for the sum of all four quark jet channels are shown in Fig. 9.

At the present time it is not completely clear what will be the real probability of a jet misidentification as a photon in CMS detector (sometimes the inverse probability of misidentification is called 'a rejection factor'). Comparing the distributions in Fig. 9 and Fig. 3-5,7 we can see that the probability of misidentification less than 10^{-3} is enough to reduce the considered background to a sufficiently small level. Probably the value of rejection factor of order of 10^4 could be realistic for the CMS detector. This value was estimated [27] after the simulation of jet fragmentation by means of PYTHIA/JETSET on the example of the subprocess $qg \to q\gamma$. Detailed simplified simulation of such kind shows that the probability for a jet with the energy E_{jet} >20 GeV to fake a photon with energy $E_\gamma > 20$ GeV is $1.6 \cdot 10^{-4}$ if both the photon and jet are observed in the detector and $1.0 \cdot 10^{-4}$ if only the photon is observed (the jet escapes the detection). For a jet with energy greater than 40 GeV these probabilities to fake a photon with energy $E_\gamma > 40$ GeV are $4.2 \cdot 10^{-4}$ and $1.8 \cdot 10^{-4}$, correspondingly.

3.4 Background processes with a gluon jet misidentified as a photon: $pp \to \gamma g + e^+\nu_e$, $pp \to \gamma g + e^-\bar{\nu}_e$

Since we cannot distinguish a gluon jet from a quark jet, these processes cannot be separated from the reactions with the quark jet considered in the previous section. The diagrams are shown in Fig. 10. The cross sections of channels with a gluon jet are several times smaller (see Table 5) and they add only slightly to the jet as misidentification a photon. Invariant mass distributions in the cases of 20 GeV and 40 GeV transverse momentum cuts for photons are shown in Fig. 11.

Double misidentification background $pp \to jj + e\nu_e$, when both jets are misidentified as photons, was estimated in [2] by means of PYTHIA. It is much smaller than the single jet misidentification backgrounds considered in this section and the previous one.

3.5 Background process with an electron misidentified as a photon: $pp \to \gamma + e^+e^-$.

The diagrams for the process of lepton pair production associated with a direct photon are shown in Fig. 12. The total cross section of the process $pp \to e^+e^- + \gamma$ with the 20 GeV cuts of transverse momenta of all final particles is equal to 0.638 pb. If we take a p_t cut at 40 GeV the cross section falls down 20 times and equals 0.029 pb. In Fig. 13 we show the $M_{\gamma l}$ invariant mass distributions which are not rising [7] at large $M_{\gamma\gamma}$ but falling rather rapidly.

Additional cut on the lepton-photon invariant mass $|M_{\gamma l} - M_Z| \geq 5$ GeV around the Z-resonance [2] does not suppress noticeably the γe^+e^- misidentification background (see Fig. 14) giving the cross section of 0.441 pb in the case $p_t^{\gamma_1,\gamma_2} \geq 20$ GeV. This is only a 30% suppression. The reason is rather evident since two s-channel Z diagrams in Fig. 12 do not give a dominant contribution to the total rate. A quark exchange in the t-channel is also an important production mechanism.

At present the probability of electron misidentification as a photon is estimated at a very small level of order of 10^{-5}. For this reason the electron misidentification background is negligible.

3.6 Background process with a b-quark misidentified as an electron: $pp \to \gamma\gamma + b\bar{b}$

We calculated the $M_{\gamma\gamma}$ distribution in the case when one of the b-quarks with low p_t escapes the detection and the other one decays semileptonically. Multiperipheral diagrams (see Fig. 15) have a singularity in the region of phase space corresponding to the forward-backward b-quark. Total cross section is 63.2 fb at the 20 GeV cut and 7.8 fb at the 40 GeV cut of photons' $p_t^{\gamma_1,\gamma_2}$. Branching ratio of the B-meson semileptonic decay $B \to l\nu_l + hadrons$ $(l = e, \mu)$ equals 0.21, and the rejection factor against the lepton originating from the b-quark is usually taken to be 10, the latter estimate follows from the experience of UA1, UA2 and CDF collaborations. So the overall factor of 0.02 appears suppressing this background to a sufficiently small level. The value of the rejection factor follows from the criteria for the B-decay lepton to be isolated. For instance, the following isolation cut could be imposed [8]: transverse momentum of the c-quark from B is less than a few GeV if $\Delta R(charm, lepton)$ <0.2. The analysis shows that the number of leptons satisfying this criterion is less than 1/10 of the whole number, leading to the rejection factor of a value more than 10.

For instance, if we are using the photonic transverse momentum cuts at 20 GeV (see Fig. 16) the rejection factor against the lepton originating from the b-quark in our case should be of order of 10-15. However, a stronger cut at 40 GeV suppresses this background by about one order of magnitude and a smaller value of rejection factor is quite enough.

4 Conclusions

Let us suppose that we can reduce all misidentification backgrounds mentioned above to a negligibly small level. For jets and leptons it does not seem difficult. Probably, the case of b-quark misidentification as a lepton will require a more careful treatment, but this background does not seem too dangerous either.

At an integrated luminosity of 165 fb^{-1} in both channels $pp \to WH$ and $pp \to t\bar{t}H$ in the two-photon invariant mass interval M_H- 1 GeV $\leq M_{\gamma\gamma} \leq M_H+$ 1 GeV we have 96 signal and 17 irreducible background events if the photon transverse momentum cuts are 20 GeV. If the photon transverse momentum cuts are taken to be 40 GeV we have 47 signal events and 1-2 irreducible background events. The Higgs peak can be observed practically free from the background. In the low luminosity regime the reaction $pp \to \gamma\gamma + lepton$ is able to produce only 4-5 clean signal events. So it can be hardly considered as a 'discovery' channel, but in the high luminosity regime it allows to fulfil an important cross-checking if the Higgs signal has shown up before in the channel $pp \to \gamma\gamma + jet$ or in the completely inclusive channel $pp \to \gamma\gamma + X$.

The calculation for $\gamma\gamma + lepton$ channel is much less sensitive to the QCD corrections and the scale uncertainties than for the $\gamma\gamma + jet$ channel [16]. However, there are significant uncertainties of reducible background cross section estimates. As in the case of the $\gamma\gamma + jet$ channel, higher two-photon invariant mass resolution could increase the significance of the signal in the final state $\gamma\gamma + lepton$, but the efficiency of photon detection that we did not take into account works in the opposite direction, reducing the number of identifiable events.

Acknowledgements

We are grateful to D. Denegri and N. Stepanov for attracting our attention to the signatures with high p_t jets. We thank very much them and S. Abdullin for the fruitful collaboration as well as E. Boos, M. Mangano and A. Pukhov for many useful discussions. We are grateful to D. Kovalenko for his collaboration in implementing the loop vertices in CompHEP. Our simulations by PYTHIA would have been impossible without the help of S. Abdullin and N. Stepanov. We are also indebted to them and I. Goloutvine, A. Nikitenko and R. Kinnunen for the interesting discussions about the CMS detector.

Our participation in the CMS Collaboration has been realized due to the kind promotion of V. Matveev and I. Goloutvine and the support of the Russian Ministry of Science and Technologies. This work was partially supported also by the European Association INTAS (grant 93-1180ext) and the Russian Foundation for Basic Research (grants 96-02-18635 and 96-02-19773).

We express our sincere gratitude to the CMS Collaboration and the CERN PPE Division for the hospitality and kind assistance during our stay at CERN.

References

[1] *Proc.of the Aachen Workshop on Large Hadron Collider*, ed. G. Jarlskog and D. Rein, CERN report 90-10, vol.II, 1990.

[2] CMS Technical Proposal, CERN/LHCC report 94-38, 1994.

[3] S.L.Glashow, D.V.Nanopoulos, A.Yildiz, Phys.Rev. **D18** (1978) 1724
P. Agrawal and S.D. Ellis, Phys. Lett. **B229** (1989) 145.

[4] Z. Kunszt, Nucl. Phys. **B247** (1984) 339.
J. Gunion et al, Nucl. Phys. **B294** (1987) 621.

[5] R. Kleiss, Z. Kunszt and W.J. Stirling, Phys. Lett. **B253** (1991) 269.

[6] Z. Kunszt, Z. Trocsanyi and W.J. Stirling, Phys. Lett. **B271** (1991) 247.

[7] S. Moretti, Cavendish preprint HEP-95/18, 1996 (hep/ph-9612310).

[8] M.L. Mangano, report SSC-SDC-90-00113, 1990.

[9] P.A. Baikov et al., in: *Proc.of X Workshop QFTHEP-95*, ed. B. Levtchenko and V. Savrin, Moscow, 1996, p.101 (hep-ph/9701412).
E.E. Boos, M.N. Dubinin, V.A. Ilyin, A.E. Pukhov and V.I. Savrin, Preprint INP MSU 94-36/358, SNUCTP 94-116, 1994 (hep-ph/9503280)

[10] V.A. Ilyin, D.N. Kovalenko and A.E. Pukhov, Int. J. Mod. Phys. **C6** (1996) 761.
D.N. Kovalenko and A.E. Pukhov, Nucl. Instrum. and Methods **389** (1997) 299.

[11] G.P. Lepage, J. Comp. Phys. **27** (1978) 192; Cornell preprint CLNS-80/447, 1980

[12] H.L. Lai et al. (CTEQ collaboration), Phys. Rev. **D51** (1995) 4763.

[13] H.L. Lai et al. (CTEQ collaboration), Phys. Rev. **D55** (1997) 1280.

[14] A.D. Martin, R.G. Roberts and W.J. Stirling. Phys. Lett. **B354** (1995) 155.

[15] M. Glück, E. Reya and A. Vogt, Z. Phys. **C53** (1992) 127.

[16] M. Dubinin, V. Ilyin, V. Savrin, in these proceedings

[17] *Review of Particle Physics*, Part I, Phys. Rev. **D54** (1996) N1.

[18] J. Ellis, M.K. Gaillard and D.V. Nanopoulos, Nucl. Phys. **B106** (1976) 292.
A.I. Vainshtein, M.B. Voloshin, V.I. Zakharov and M.A. Shifman, Sov. J. Nucl. Phys. **30** N5 (1979) 711.
E. Eichten, I. Hinchliffe, K. Lane and C. Quigg, Rev. Mod. Phys. **56** (1984) 579; Rev. Mod. Phys. **58** (1985) 1065.
L.B. Okun, *Leptons and Quarks*, North Holland, 1984.

[19] S.G. Gorishny, A.L. Kataev, S.A. Larin and L.R. Surguladze, Mod. Phys. Lett. **A5** N32 (1990) 2703.
N. Gray, D.J. Broadhurst, W. Grafe and K. Schilcher, Z. Phys. **C48** (1990) 673.
A.L. Kataev and V.T. Kim, Mod. Phys. Lett. **A9** N14 (1994) 1309.

[20] J. Fleischer and F. Jegerlehner, Phys. Rev. **D23** (1981) 2001.
D.Yu. Bardin, B.M. Vilenski and P.Kh. Khristova, Sov. J. Nucl. Phys. **53** (1991) 152.
A. Dabelstein and W. Hollik, Z. Phys. **C53** (1992) 507.
B.A. Kniehl, Nucl. Phys. **B376** (1992) 3.

[21] A. Djouadi, M. Spira and P.M. Zerwas, Phys. Lett. **B264** (1991) 440.

[22] M. Spira, A. Djouadi, D. Graudenz and P.M. Zerwas, Nucl. Phys. **B453** (1995) 17.

[23] K.G. Chetyrkin, B.A. Kniehl and M. Steinhauser, MPI/PhT/97-006; hep-ph/9705240.

[24] A. Djouadi and P. Gambino, Phys. Rev. Lett. **73** (1994) 2528.
Y. Liao and X. Li, hep-ph/9605310.

[25] T.G. Rizzo, Phys. Rev **D22** (1980) 722.

[26] M. Spira, DESY T-95-05; hep-ph/9510347.
A. Djouadi, J. Kalinowski and M. Spira, DESY 97-079; hep-ph/9704448.
M. Spira, Nucl. Instrum. and Methods **389** (1997) 357.

[27] S. Abdullin, private communication

$p_t^{\gamma_1}$,GeV	-	20	40	40		40	40	40
$p_t^{\gamma_2}$,GeV	-	20	20	40		20	20	20
p_t^e, GeV	-	20	20	20		20	20	10
$\Delta R(\gamma, e)$	-	0.3	0.3	0.3		0.2	0.3	0.3
$\eta_{\gamma,e}$	-	2.4	2.4	2.4		2.4	3.0	2.4
$\sigma(pp \to \gamma\gamma e^-\bar{\nu}_e) \cdot 10^5$ (pb)								
	14.28	6.08	5.85	2.73		5.89	7.47	6.41
$\sigma(pp \to \gamma\gamma e^+\nu_e) \cdot 10^5$ (pb)								
	24.45	9.23	8.90	4.33		9.08	12.32	10.03
signal events in both $e^+\nu_e, e^-\bar{\nu}_e$ channels, $L = 1.65 \cdot 10^5\ pb^{-1}$								
	64	25	24	12		25	33	27
signal events in the $e\nu_e$, $\mu\nu_\mu$ channels								
	128	50	48	24		50	66	54
background events in $e\nu_e$, $\mu\nu_\mu$ channels, $\Delta M_{\gamma\gamma} = 1$ GeV								
		14	10	1		12	16	12
significance of the signal								
		13.4	15.2	24		14.4	16.5	15.6

Table 1: Signal cross sections and the number of signal events at the integrated luminosity of $1.65 \cdot 10^5$ pb^{-1} in the channels $\gamma\gamma l\nu_l$ ($l = e^+, e^-$ and μ^+, μ^-) for various sets of kinematical cuts. Standard set of cuts that was used in the CMS Technical Proposal [2] is shown in the fourth column. Signal significance in the interval $M_H - 1$ GeV $< \Delta M_{\gamma\gamma} < M_H + 1$ GeV is defined as $S = N_S/\sqrt{N_B}$, where N_S and N_B are the numbers of signal and background events.

$p_t^{\gamma_1}$, GeV	$p_t^{\gamma_2}$, GeV	$\sigma \cdot 10^4$, pb
$ud \to \gamma\gamma e^+ \nu_e$		
20	20	23.2
40	20	15.5
40	40	5.3
$\bar{u}d \to \gamma\gamma e^- \bar{\nu}_e$		
20	20	16.1
40	20	10.6
40	40	3.3

Table 2: Total cross sections for the signal and irreducible background diagrams (Fig. 10) with various photon p_t cuts. Standard cuts $p_t^e > 20$ GeV, $|\eta_\gamma| < 2.4$, $|\eta_e| < 2.4$, $\Delta R = \sqrt{\Delta\varphi^2 + \Delta\eta^2} > 0.3$ for the rapidity range and the lepton (photon) separation are used.

$p_t^{\gamma_1}$, GeV	$p_t^{\gamma_2}$, GeV	$\sigma \cdot 10^4$, pb
$gg \to \gamma\gamma t\bar{t}$		
20	20	56.4
40	20	50.3
40	40	24.0

Table 3: Total cross sections for the signal and irreducible background diagrams (see the signal in Fig. 15 and the irreducible background in Fig. 24 with the replacement $b \to t$) with various photon p_t cuts. No cuts are imposed on the t-quark. Standard cuts $p_t^e > 20$ GeV, $|\eta_\gamma| < 2.4$, $|\eta_e| < 2.4$, $\Delta R > 0.3$ for the rapidity range and the lepton (photon) separation are used.

$p_t^{\gamma_1}$, GeV	$p_t^{\gamma_2}$, GeV	σ, pb
$gu \to \gamma d e^+ \nu_e$		
20	20	0.81
40	20	0.64
40	40	0.26
$g\bar{u} \to \gamma \bar{d} e^- \bar{\nu}_e$		
20	20	0.57
40	20	0.43
40	40	0.15
$g\bar{d} \to \gamma \bar{u} e^+ \nu_e$		
20	20	0.35
40	20	0.25
40	40	0.09
$gd \to \gamma u e^- \bar{\nu}_e$		
20	20	0.96
40	20	0.77
40	40	0.28
sum of all channels with quark jet		
20	20	2.69
40	20	2.10
40	40	0.77

Table 4: Total cross sections of four channels for the background when the quark jet is misidentified as a photon. Three sets of p_t cuts are used for γ and q. Standard cuts are $p_t^e > 20$ GeV, $|\eta_\gamma| < 2.4$, $|\eta_e| < 2.4$, $\Delta R > 0.3$ for the lepton rapidity range and the lepton (photon) separation.

$p_t^{\gamma_1}$, GeV	$p_t^{\gamma_2}$, GeV	σ, pb
$u\bar{d} \to \gamma g e^+ \nu_e$		
20	20	0.30
40	20	0.20
40	40	0.06
$\bar{u}d \to \gamma g e^- \bar{\nu}_e$		
20	20	0.45
40	20	0.27
40	40	0.09

Table 5: Total cross sections of two channels for the background when the gluon jet is misidentified as a photon. Three sets of p_t cuts are used for γ and q. Standard cuts are $p_t^e > 20$ GeV, $|\eta_\gamma| < 2.4$, $|\eta_e| < 2.4$, $\Delta R > 0.3$ for the rapidity range and the lepton (photon) separation.

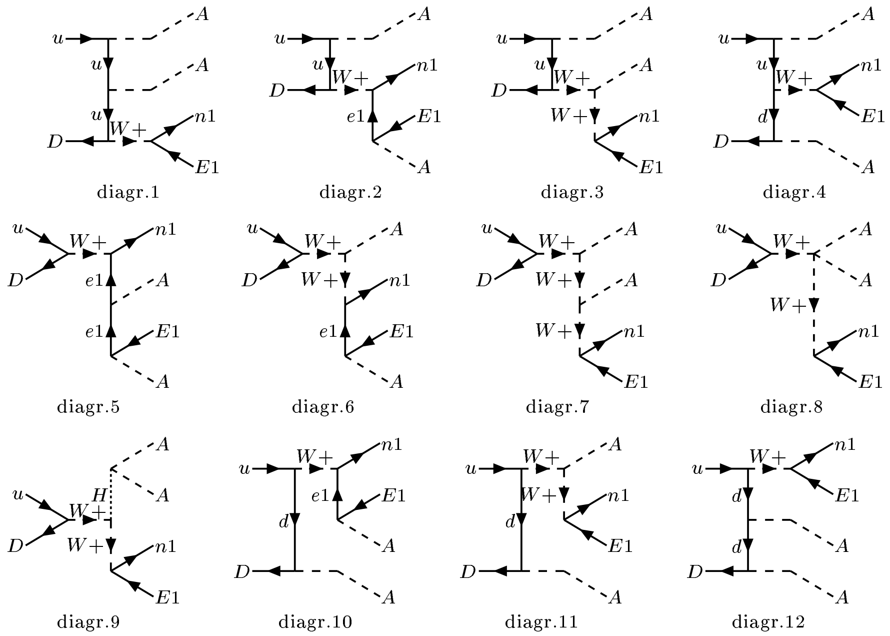

Figure 1: Feynman diagrams (unitary gauge) for the process $pp \to \gamma\gamma e^+\nu_e$. CompHEP notation $A = \gamma$, $e1 = e^-$, $E1 = e^+$, $n1 = \nu_e$, $D = \bar{d}$ is used.

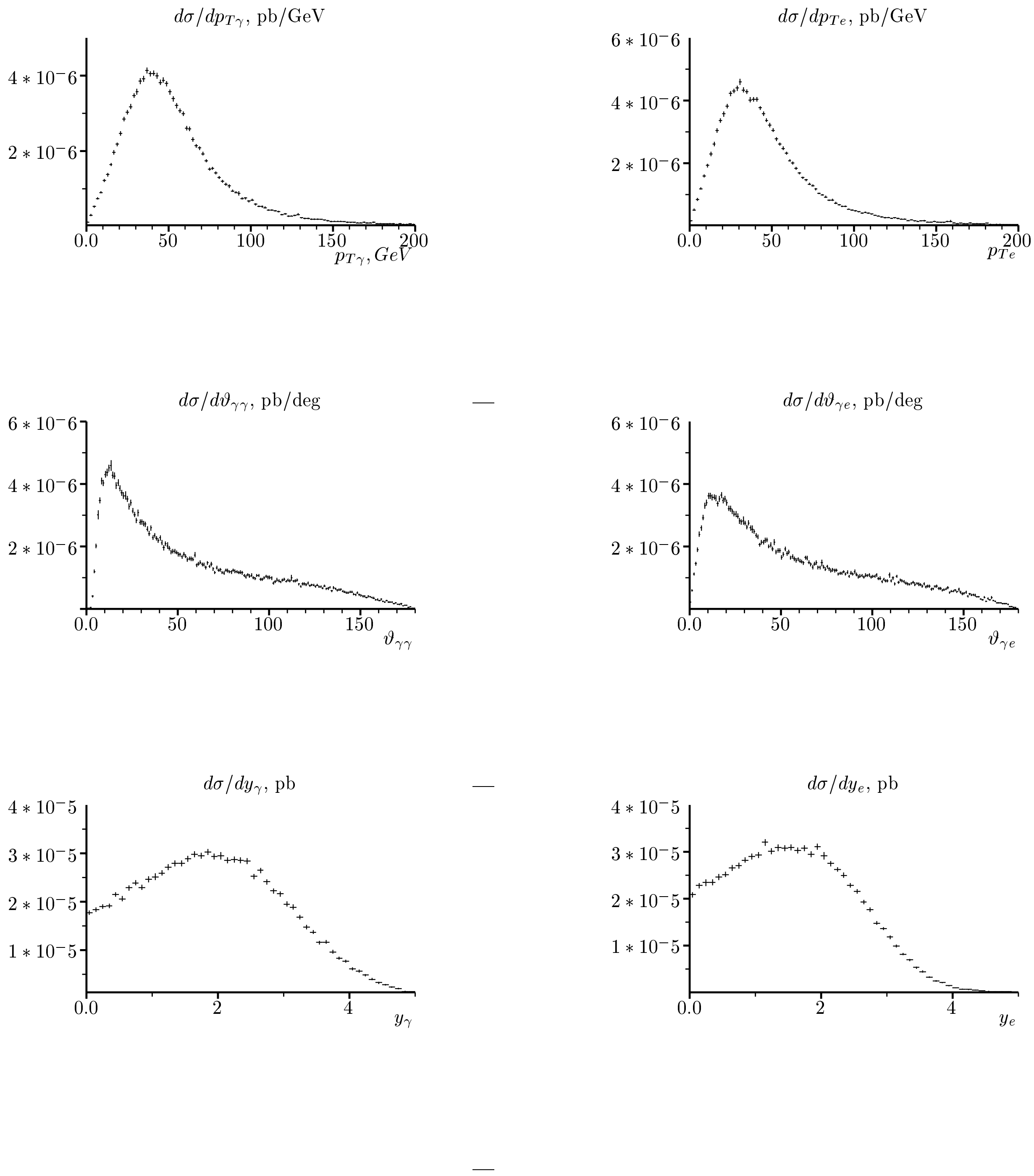

Figure 2: Distributions in $p_t^{\gamma}, p_t^{e}, \eta_{\gamma}, \eta_e, \vartheta_{\gamma\gamma}, \vartheta_{\gamma e}$ for the process $pp \to \gamma\gamma e^+\nu_e$ with account of the signal diagram (number 9 in Fig. 10) only. No kinematical cuts are applied.

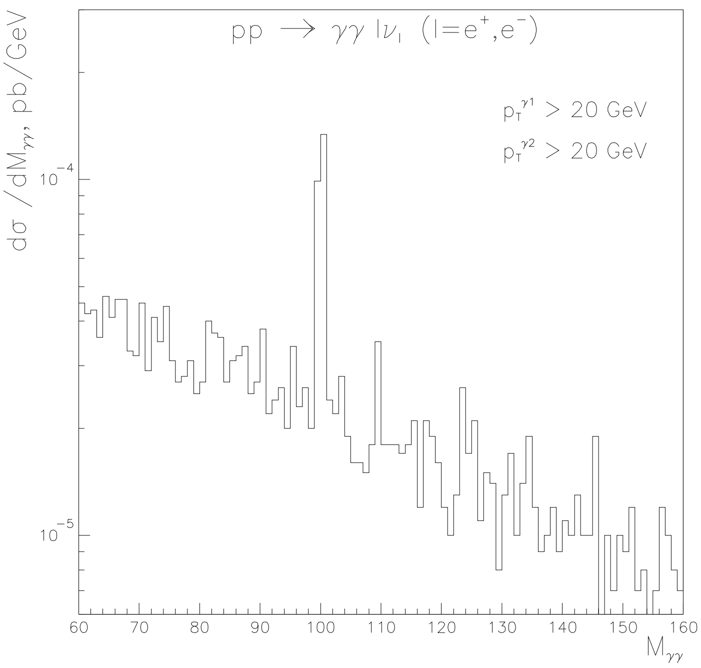

Figure 3: Distribution in $M_{\gamma\gamma}$ for the process $pp \to \gamma\gamma + l\nu_l$ ($l = e^+$ and e^-) with account of the signal and irreducible background (see 12 diagrams in Fig. 12). Photonic transverse momentum cuts $p_t^{\gamma_1} > 20$ GeV, $p_t^{\gamma_2} > 20$ GeV. Electron transverse momentum cut $p_t^e > 20$ GeV, lepton pseudorapidity cuts $|\eta_\gamma| < 2.4$, $|\eta_e| < 2.4$, lepton (photon) separation cuts $\Delta R = \sqrt{\Delta\varphi^2 + \Delta\eta^2} > 0.3$. Here and in the following we are using the parton distribution functions CTEQ3m at the scale $Q^2 = M_H^2$.

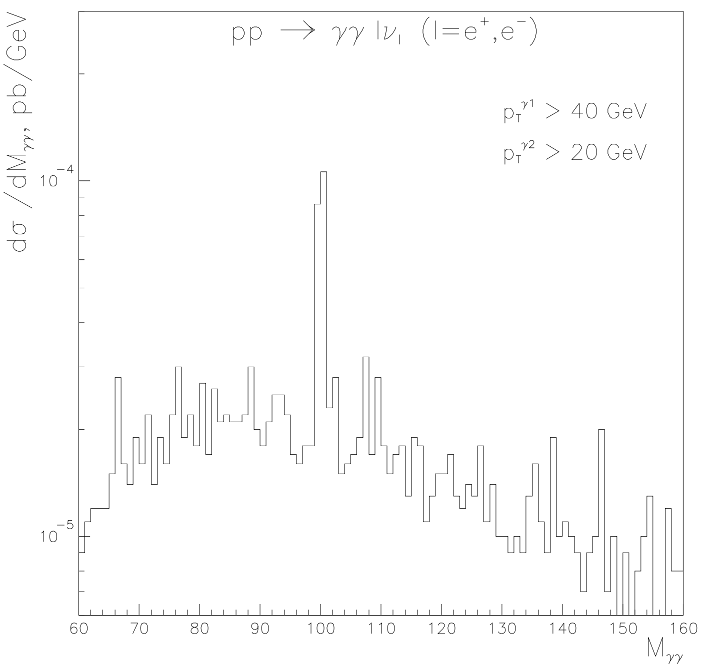

Figure 4: The same as in Fig.12 for photonic transverse momentum cuts $p_t^{\gamma_1} > 40$ GeV, $p_t^{\gamma_2} > 20$ GeV.

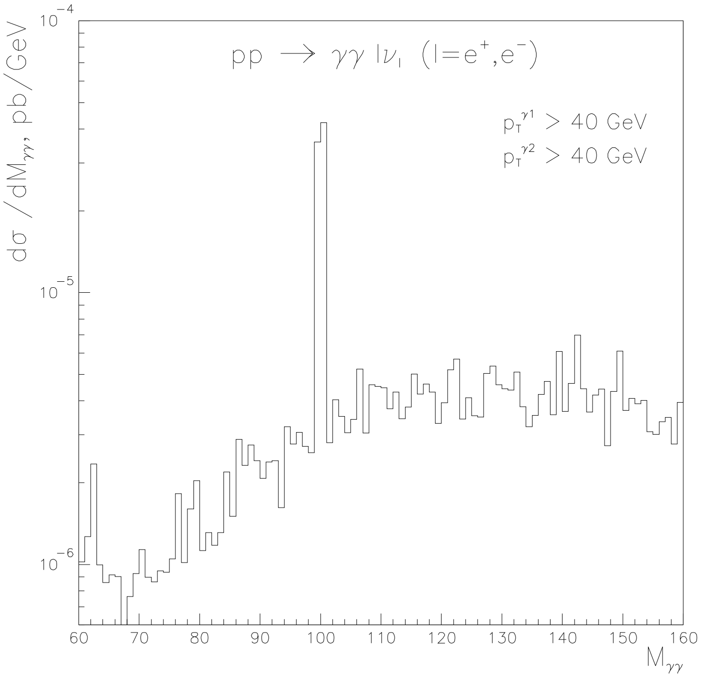

Figure 5: The same as in Fig.12 for photonic transverse momentum cuts $p_t^{\gamma_1} > 40$ GeV, $p_t^{\gamma_2} > 40$ GeV.

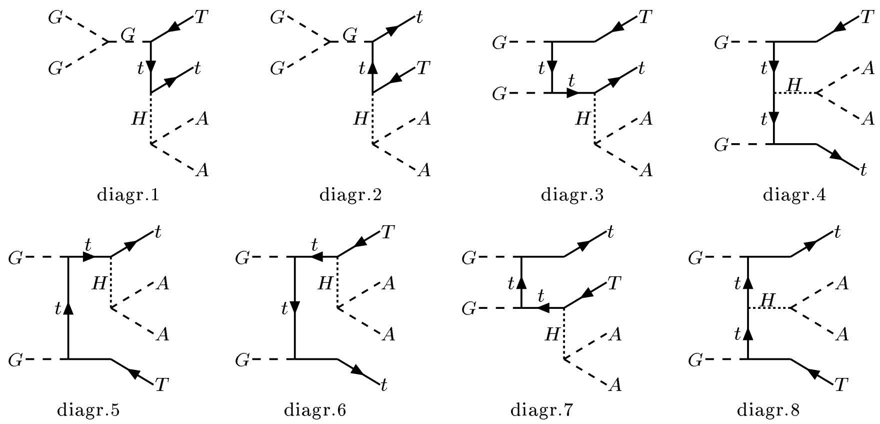

Figure 6: Signal diagrams for the process $pp \to \gamma\gamma + t\bar{t}$

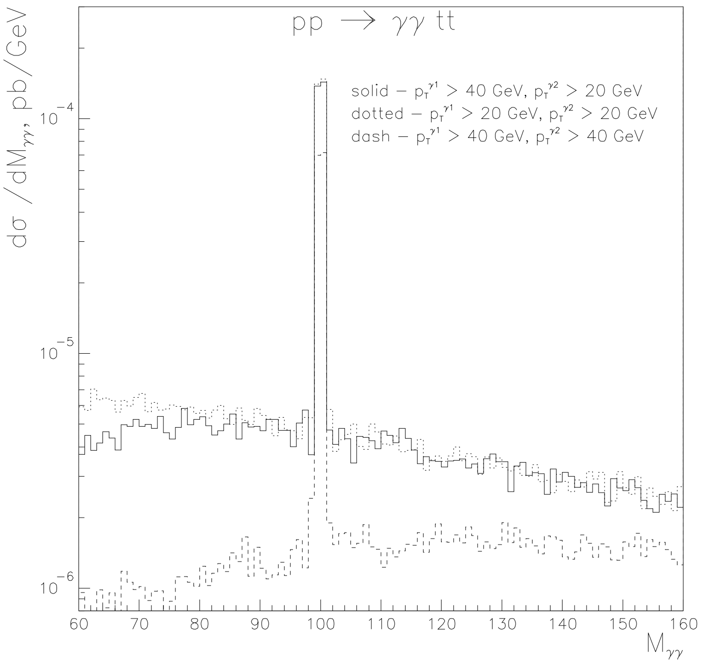

Figure 7: Distribution in $M_{\gamma\gamma}$ the signal (Fig.15) and irreducible background (see Fig.24, $b \to t$) diagrams of the process $pp \to \gamma\gamma + t\bar{t}$. No cuts are imposed on the t-quarks. We suppose one (and only one) lepton from the $t\bar{t}$ state to be detected, the displayed distribution is already multiplied by $2 \times Br^2(t \to Wb) * Br(W \to qq)$ and $Br(W \to l\nu_l)$ $(l = e, \mu)$. Standard cuts for photons: $|\eta_\gamma| < 2.4$, $\Delta R > 0.3$, $p_t^\gamma >$ 20 or 40 GeV.

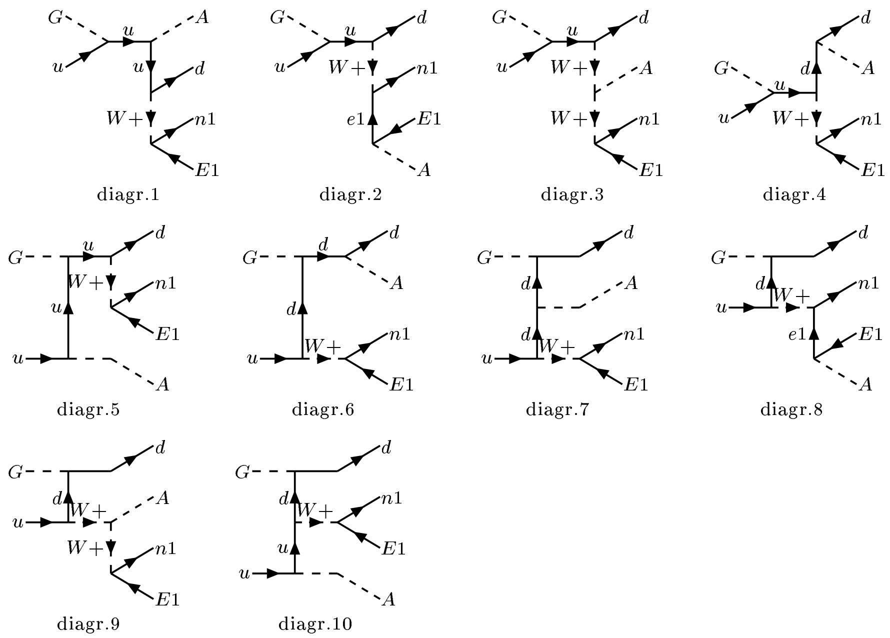

Figure 8: Feynman diagrams for the background process $pp \to \gamma d e^+ \nu_e$

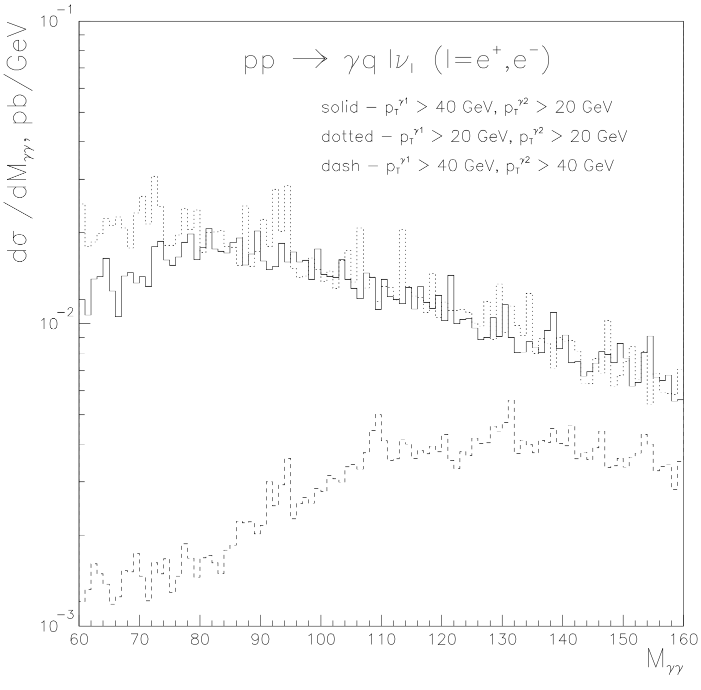

Figure 9: Distribution in $M_{\gamma q}$ for the sum of all channels of quark misidentification as a photon. Transverse momentum cuts for the direct photon and the photon from the quark jet: $p_t^{\gamma_1} > 40$ GeV, $p_t^{\gamma_2} > 20$ GeV (solid line), $p_t^{\gamma_1} > 20$ GeV, $p_t^{\gamma_2} > 20$ GeV (dotted line), $p_t^{\gamma_1} > 40$ GeV, $p_t^{\gamma_2} > 40$ GeV (dash line). Standard cuts are $p_t^e > 20$ GeV, $|\eta_\gamma| < 2.4$, $|\eta_e| < 2.4$, $\Delta R > 0.3$ for the lepton rapidity range and the lepton (photon) separation.

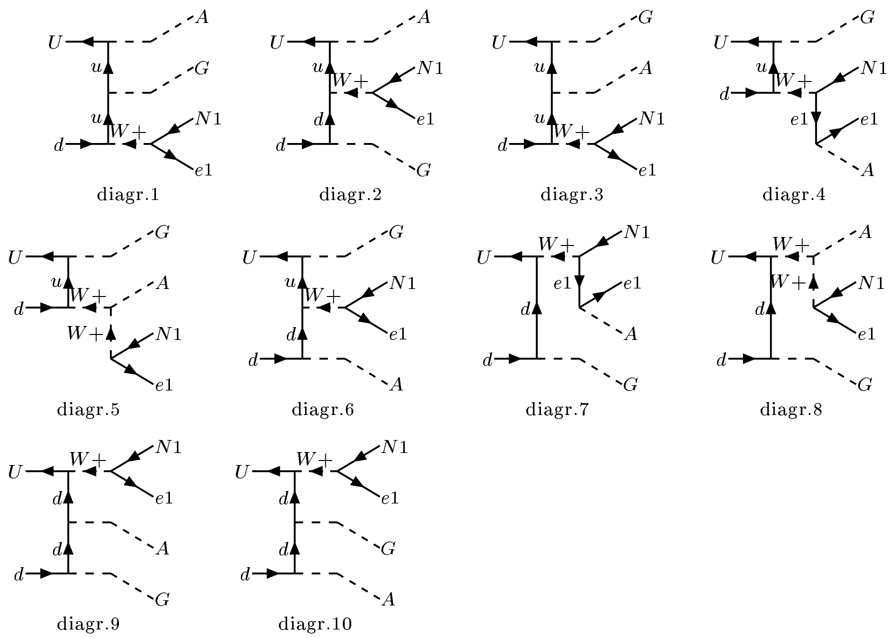

Figure 10: Feynman diagrams for the background process $u\bar{d} \rightarrow \gamma g e^{+} \nu_e$

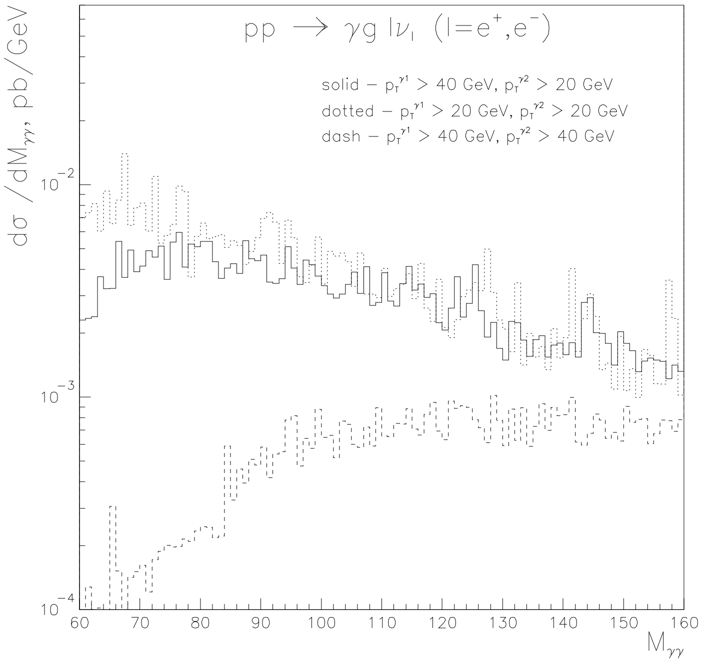

Figure 11: Distribution in $M_{\gamma g}$ for the sum of all channels of gluon jet misidentification as a photon. Transverse momentum cuts for the direct photon and the photon from the gluon jet: $p_t^{\gamma_1} > 40$ GeV, $p_t^{\gamma_2} > 20$ GeV (solid line), $p_t^{\gamma_1} > 20$ GeV, $p_t^{\gamma_2} > 20$ GeV (dotted line), $p_t^{\gamma_1} > 40$ GeV, $p_t^{\gamma_2} > 40$ GeV (dash line). Standard cuts are $p_t^e > 20$ GeV, $|\eta_\gamma| < 2.4$, $|\eta_e| < 2.4$, $\Delta R > 0.3$ for the lepton rapidity range and the lepton (photon) separation.

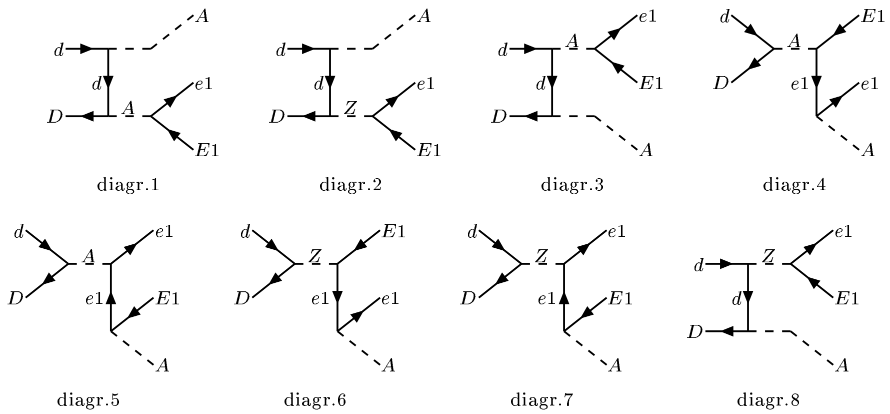

Figure 12: Feynman diagrams for the background process $u\bar{u} \to \gamma e^+ e^-$

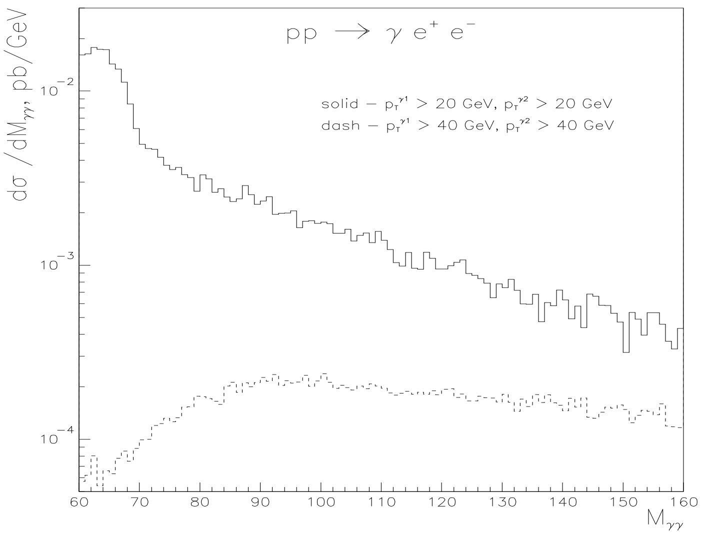

Figure 13: Distribution in $M_{\gamma e}$ for the process $pp \to \gamma e^+e^-$. Transverse momentum cuts of the direct photon and the photon from the electron misidentification are $p_t^{\gamma_1} > 20$ GeV, $p_t^{\gamma_2} > 20$ GeV for the solid line, and $p_t^{\gamma_1} > 40$ GeV, $p_t^{\gamma_2} > 40$ GeV for the dash line. Standard cuts are $p_t^{e,\gamma} > 20$ GeV, $|\eta_\gamma| < 2.4$, $|\eta_e| < 2.4$, $\Delta R > 0.3$ for the lepton rapidity range and the lepton (photon) separation.

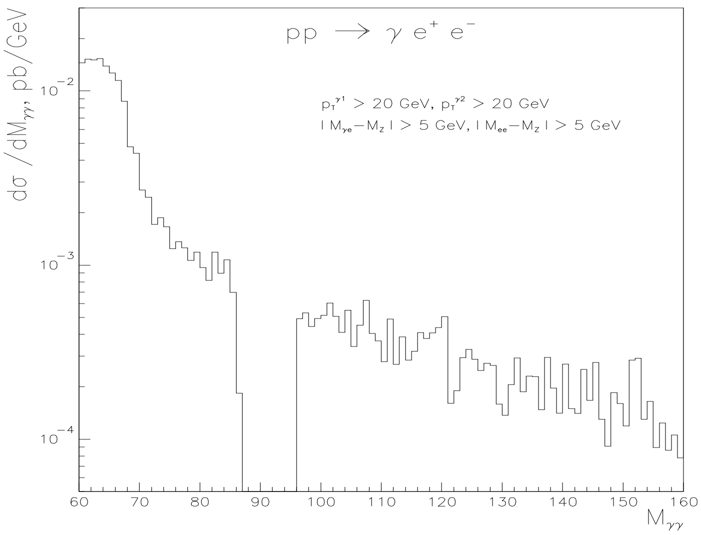

Figure 14: The same as in Fig. 22 ($p_t^{\gamma_{1,2}} > 40$ GeV) with the additional cut around the Z resonance $|M_{\gamma e} - M_Z| > 5$ GeV, $|M_{e^+e^-} - M_Z| > 5$ GeV.

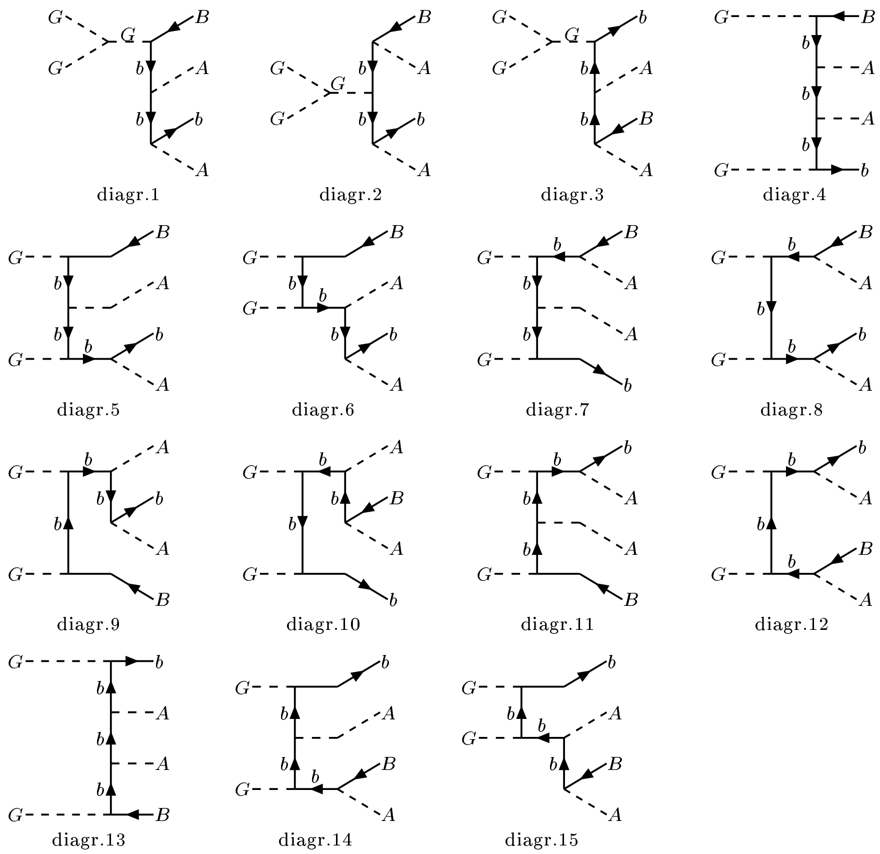

Figure 15: Feynman diagrams for the background process $gg \to \gamma\gamma b\bar{b}$

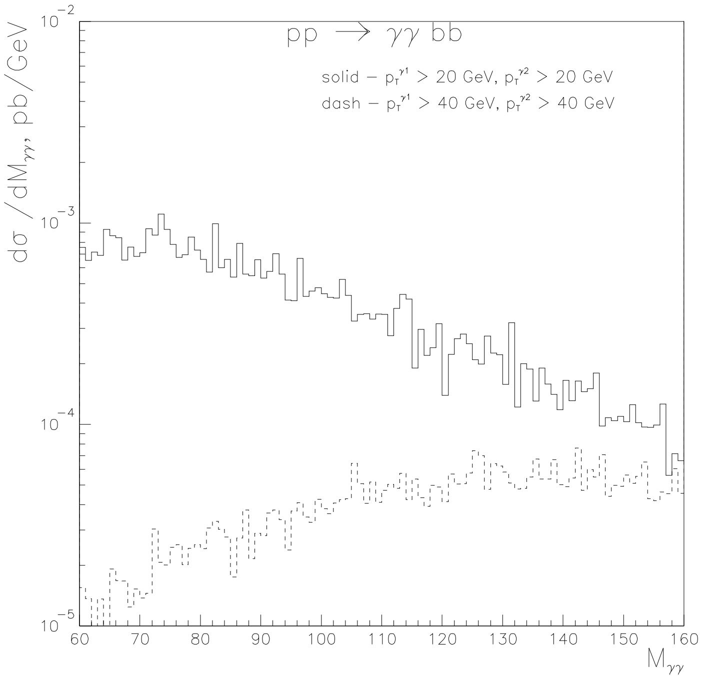

Figure 16: DIstribution in $M_{\gamma\gamma}$ for the background process $pp \to \gamma\gamma b\bar{b}$, transverse momenta cuts for both photons are 20 or 40 GeV.